International Journal of Technology 14(5) 1134-1146 (2023)
Received October 2022 / Revised November 2022 / Accepted December 2022

International Journal of Technology

http://ijtech.eng.ui.ac.id

Development of Zirconia Reinforced AA7075/AA7050 Aluminum Chip-Based Composite Processed Using Hot Press Forging Method

Yahya M. Altharan[1], S Shamsudin[1*], Sam. Al-Alimi[1], Mohammed A. Jubair[2]

[1]*Sustainable Manufacturing and Recycling Technology, Advanced Manufacturing and Materials Center (SMART-AMMC), Universiti Tun Hussein Onn Malaysia, Parit Raja 86400, Malaysia*
[2]*Department of Computer Technical Engineering, College of Information Technology, Imam Ja'afar Al-Sadiq University, 66002 Al-Muthanna, Iraq*

Abstract. The solid-state recycling technique has gained significant attention for its ability to reduce metal losses, energy consumption, and solid waste. This study introduced solid-state recycling method to develop zirconia-reinforced AA7075/AA7050 aluminum chip-based matrix composite via a hot press forging process (HPF). The chips were cold-compacted at 35 tons and then hot-forged through a dog bone-shaped die. Full factorial and response surface methodology (RSM) designs were applied using Minitab 18 software. The Face Centred Composite (CCF) of RSM was adopted to rank each factor's effect and analyze interactions between input factors and output responses, followed by process optimization. The selected factors of temperature (Tp) and volume fraction of zirconia (ZrO_2) nanoparticles (Vf) were set at 450, 500, and 550 °C with 5, 10, and 15 wt %, respectively. The analyzed responses were ultimate tensile strength (UTS) and microhardness (MH). SEM micrograph revealed a slightly uniform distribution of ZrO_2 particles in the matrix. The developed composite gained the maximum strength of 262.52 MPa, a microhardness of 135.5 HV and a density of 2.828 g/cm^3 at 550 °C and 10 wt % setting. RSM optimization results suggested 550 °C and 10.15 wt % as optimal conditions for maximum UTS and MH. The preheating temperature exhibited a more significant influence than the ZrO_2 volume fraction on the composite's mechanical properties; however, both had a slight effect on grain size. The future prospects of this work are briefly addressed at the end. In conclusion, the HPF process was found to be an efficient recycling method for mitigating environmental impacts by conserving energy and materials.

Keywords: Composite, Mechanical properties, Microstructure, Recycling

1. Introduction

Aluminum alloys are the most commonly used materials in automotive and aerospace structures due to their lightweight properties and enhanced fuel efficiency to reduce CO_2 emissions (Rana, Purohit, and Das, 2012). However, the intensive industrial production of aluminum due to high demands caused negative environmental impacts such as CO_2 emissions and large amounts of solid waste (Agboola *et al.*, 2020). According to the International Aluminum Institute, the primary aluminum industry is accountable for 1.1% billion tonnes of total CO_2 emissions due to smelting processes (International Aluminium Institute, n.d.). In detail, 60% of the indirect emissions come from electric power generation and 40% come from the aluminum production processes. Primary aluminum production

*Corresponding author's email: shazarel@uthm.edu.my, Tel: +60136923896
doi: 10.14716/ijtech.v14i5.6032

(mining from bauxite ore) requires 113 GJ of energy per tonne, while secondary production (recycling) needs just 13.6 GJ per tonne (Cui and Roven, 2010). This substantial decrease in energy consumption encourages aluminum scrap recycling instead of disposal.

The considerable amounts of scrap and chips generated during machining are able to be recycled and repurposed to achieve sustainability. Numerous researchers have studied aluminum waste recycling to save energy and reduce environmental issues (Yong *et al.*, 2019; Keoleian and Sullivan, 2012). However, recycling aluminum by remelting still consumes high energy and emits CO_2, according to some studies (Yong *et al.*, 2019; Wan *et al.*, 2017; Rana, Purohit, and Das, 2012). Meanwhile, other research indicated that converting chips and scraps into semi-product without remelting is eco-friendly since it utilizes 95% less energy and emits just 5% of the greenhouse gas than the primary production process (International Aluminium Institute, n.d.; Shamsudin, Lajis, and Zhong, 2016). Hot press forging (HPF) is a preferred conversion recycling method for chip-based products with good mechanical and physical properties (Lajis, Yusuf, and Ahmad, 2018). Therefore, this work proposes HPF as a novel direct recycling technique for secondary aluminum production.

In the current research, AA7075/AA7050 chip was recycled through HPF and reinforced by zirconia particles (ZrO_2) with an average size of 3 µm. ZrO_2-nanoparticle was chosen due to its mechanical properties, high-temperature stability, wear, corrosion, and chemical resistance (Parveen, Chauhan, and Suhaib, 2019). Incorporating ZrO_2 particles in aluminum chips improve the tensile strength and hardness of aluminum metal matrix composites (AMCs) (Reddy *et al.*, 2020). The characteristics AMCs are determined by the interface between the reinforcement and the matrix (Srivyas and Charoo, 2018). AMCs combine the good properties of matrix metal (high ductility and low density) and ceramics (high modulus and strength). However, developing quality-effective and satisfactory end products of AMCs with fundamental geometrical remains a significant challenge. When recycling composite, experimental factors like processing temperature, cold compaction, matrix morphology, and reinforcement material must be well-designed. Design of experiment (DOE) is an efficient technique to investigate the effect of different factors and determine the optimum parameters. In multifactorial experiments, optimization is typically conducted by varying a single factor while all other factors are fixed at a particular set of conditions (Jankovic, Chaudhary, and Goia, 2021). It is not just time-consuming but also unable to determine the true optimum as it neglects the interactions among the variables. Hence, DOE was used to design the process parameters and study the influence of input factors on responses via response surface methodology (RSM) using Minitab 18 software. Analysis of variance (ANOVA) was also adopted to determine the significant parameters influencing responses and reveal optimal design with desired mechanical and physical properties. Besides the microstructural examination, composite samples were tested for ultimate tensile strength (UTS), yield strength (YS), elongation at break (EAB), and microhardness (MH). Tensile strength and microhardness were the qualitative responses to be optimized based on the effect of optimal input factors.

This research aims to recycle AA7075/AA7050 aluminum chip by HPF and investigate the influence of preheating temperatures and ZrO_2 addition on the mechanical and physical properties of the forged composite. The developed composite material was able to be used in the transportation industry. However, the profile quality is able to be improved by heat treatment. This research has a tendency to contribute to further attention toward direct recycling technologies to conserve energy and natural resources.

2. Methods

2.1. Materials Preparation

The materials used, such as aluminum chips and zirconia reinforcement material, were supplied by SMART-AMMC, UTHM. The chips were produced from AA7075/AA7050 aluminum bulk with 3.30 × 1.12 × 0.095 mm average size using Sodick-MC430L high-speed milling. The chip was cleaned using acetone (C3H6O) in an ultrasonic bath based on ASTM G131-96 and then dried at 60 °C for 30 min. The prepared chips were mixed with zirconia nanoparticles averaging 3 μm in size using a 3D mixer.

2.2. Rule of Mixing

The aluminum chip and reinforcement particles were mixed to develop uniform distribution throughout the composite. The density-based mixtures rule method was used to determine the required amount of chips and zirconia nanoparticles for the composite production, as presented in the following equations:

$$\rho = \frac{m}{v} \tag{1}$$

$$\rho_c = \rho_z V_z + \rho_m V_m \tag{2}$$

$$m_c = \rho_c V_c \tag{3}$$

$$V_c = L \times W \times h \tag{4}$$

Where ρ_c is composite's density, V refers to volume with subscripts z and m for zirconia nanoparticles and metal matrix, respectively. The m_c and V_c are the mass and volume of the composite, respectively. The corresponding volume fraction is calculated by the given relation:

$$V_f = \frac{\left(\frac{M_\rho}{P_\rho}\right)}{\left(\frac{m_\rho}{P_\rho}+\frac{M_m}{P_m}\right)} \tag{5}$$

Where V_f is the volume fraction of particles. M_m and Pρ are mass and density of the particles and matrix, respectively.

2.3. Experimental Design

Design of experiments (DOE) was used to determine the influence of significant factors and their interactions to optimize the responses via RSM. The input factors were temperature (Tp: 450, 500, and 550 °C) and ZrO_2 (Vf: 5, 10, and 15 wt %). The UTS and MH responses of the forged composite were investigated by varying the input factors. To analyze the influence of different settings of Tp and Vf on UTS and MH, the 2^k full factorial design (k is number of factors) with 2 replicates and 3 center points for curvature effect analysis was chosen as it is very useful in screening the significant factors of the experiment. Eleven runs were involved, corresponding to the experimental design selected and the run scheme given in Table 1. The star points correspond to α value of 1 to evaluate the interaction between the parameters. RSM was used to obtain the optimal setting that resulted in the highest UTS and MH. The model's regression general equation (6) determines the correlation between the dependent (responses) and independent variables (input factors).

$$y = b = b_0 + b_1 X_1 + b_2 X_2 + \cdots + b_k X_k \tag{6}$$

Where y is dependent variable, b_0 is constant, b_1 , b_1 , ..., b_k are coefficient and X_1 , X_2 , ... X_k are the independent variables.

Table 1 Design scheme of the process parameters (uncontrolled variables)

Factor symbol	Parameter	Levels		
		Low (−1)	Centre (0)	High (+1)
T_p	Preheating temp. (°C)	450	500	550
V_f	Vol. fraction of ZrO_2 (wt %)	5	10	15

2.4. *Hot Press Forging Process (HPF)*

The mixture of chip and ZrO_2 particles was weighed at 14 g as per the rule of mixing result and filled up into Flat-Face dog bone-shaped die in Figure 1(a), then cold compacted at 35 tons and four times pre-compacting cycle. The billet die was preheated for 45 min of homogenization time at the desired temperature followed by 2 hours of holding time and forging temperatures (Tp) of 450–550 °C, between the solidus and recrystallization point.

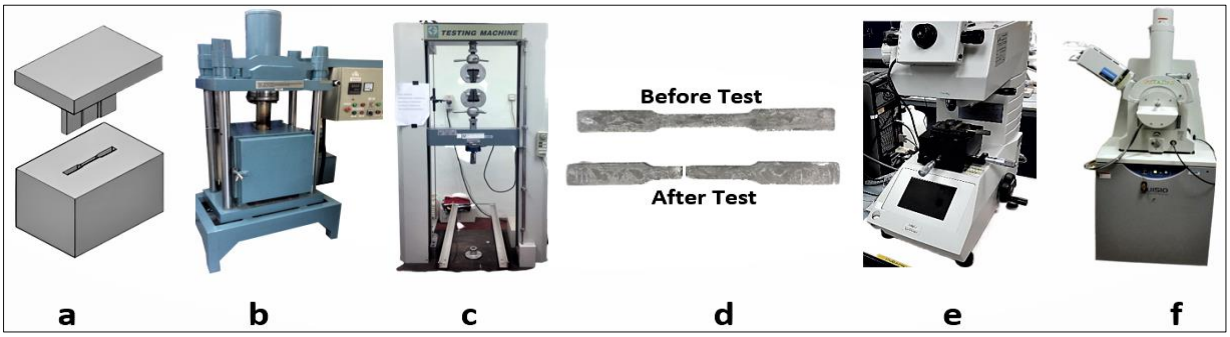

Figure 1 (a) Top and bottom forging die, (b) Forging machine, (c) Tensile testing machine, (d) Forged specimens, (e) Hardness tester and (f) SEM microscope

2.5. *Experimental Tests*

The exact geometric dimensions of specimens were based on ASTM E8/E8M (Figure 2). The tensile test of samples was performed using a universal testing machine (Shimadzu EHF-EM0100K1-020-0A). The hardness specimens were tested by Vickers microhardness tester, under a predetermined force of 2.943 N load for 10 s (ASTM E384-11). Microstructure tests were conducted utilizing a scanning electron microscope SEM-JSM T330. The fracture surface morphology was examined by SEM Hitachi SU1510 based on Standard ASTM E3 and ASTM E340 through an optical microscope (Olympus BX60M). The testing specimens were ground using 240, 600, and 1200 SiC paper for 3 min, polished to 6 µm TEXPAN, 1 and 2 µm NAPPAD for 540 s each, then etched at 12 V DC for 2 minutes by Barker's reagent. The density test was carried out in distilled water for whole specimens using HR-250AZ-Compact Analytical Balance Density Determination Kit. Small billet specimens were weighed in air and distilled water to record the weight in various environments. The room temperature was recorded to calculate the relative density by using the following equation:

$$\rho = \frac{m}{|V|} \times density\ of\ distilled\ water\ at\ a\ certain\ temperature \quad (7)$$

Where **ρ**, m, and V are density, mass on air, and volume in liquid, respectively.

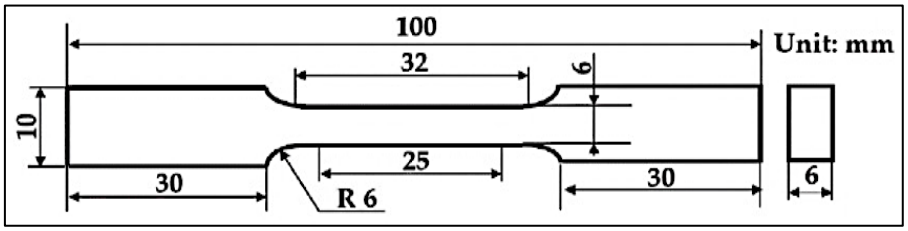

Figure 2 Plate-type Tension Test Specimen (ASTM E8M) (ASTM E8/E8M-21, 2022)

Table 2 The chemical composition of AA7075/7075 (*ASTM B221M -13, 2015,354)*

Element (%)	*Si*	*Fe*	*Cu*	*Mn*	*Mg*	*Zn*	*Cr*	*Ti*
AA7075	0.4 Max	0.5 Max	1.2–2	0.3 Max	2.1–2.9	5.1–6.1	0.18–0.28	0.2 Max
AA7050	0.12 Max	0.15 Max	2–2.6	0.10 Max	1.9–2.6	5.7–6.7	0.04 Max	0.06 Max

3. Results and Discussion

3.1. Ultimate Tensile Strength (UTS)

The UTS results with different temperatures and ZrO_2 volume fractions, including four additional experiments suggested by DOE for process optimization are shown in Table 3. UTS increased by 288.13% from 56.94 to 221 MPa for 550 °C-forged samples (S1) and 450 °C-forged samples (S2), despite both two samples being reinforced by 5 wt % ZrO_2 particles. The UTS of S2 and S13 embedded with 5 and 10 wt % and 550 °C-forged increased by18.78% from 221 MPa to 262.52 MPa. The composite's dislocation density exceeded that of the zirconium oxide nanoparticles. In metal deformation, the strength increases linearly with dislocation density (S. Al-Alimi *et al.*, 2020a). The UTS of the composites increased up to 10 wt% of ZrO_2. However, deteriorated by increasing ZrO_2 weight content to 15 %, as recorded in samples S4 and S8. This is because a higher volume fraction of ZrO_2 caused particle agglomeration and availability of pores. However, low ZrO_2 content diffusion was not enough to destruct the oxide layer, causing partial disruption in an immature state of chip consolidation (Al-Alimi *et al.*, 2022).

The findings show that the UTS was high at 550 °C with different wt % of ZrO_2. The higher operating temperature above the solidus point resulted in good metallic bonding between consolidated chips. High processing temperature and average weight content of ZrO_2 resulted in relatively recrystallized grains, where grain coarsening was metallurgically bonded (Sabbar *et al.*, 2021). Sample S13 (90% chips + 10 wt % ZrO_2) that forged at 550 550 °C had the highest UTS of 262.521 MPa. The UTS of this sample (S13) increased 23.18% compared to S16 (100% chip). This was agreed by (Al-Alimi *et al.*, 2022; Reddy *et al.*, 2020) that ZrO_2 enhances the UTS of recycled MMCs. Experimentally, UTS increases linearly with forging temperature and ZrO_2 content 10 wt % addition.

Table 3 Results of Elongation at Break, Yield strength, UTS, and MH tests for all samples

Sample No.	Inputs Factors		Output Responses			
	Temp. (°C)	ZrO_2 (%)	EAB (mm)	YS (MPa)	UTS (MPa)	MH (HV)
S1	450	5	0.760	55.88	56.94	80.600
S2	550	5	1.777	221.0	221.0	111.57
S3	450	15	1.283	53.35	58.22	83.500
S4	550	15	1.274	178.8	240.0	121.70
S5	450	5	0.619	63.78	64.00	84.100
S6	550	5	1.954	232.7	238.9	114.70
S7	450	15	1.134	44.90	48.40	76.20
S8	550	15	3.083	220.4	254.0	130.20
S9	500	10	1.460	126.0	191.7	122.50
S10	500	10	1.510	143.6	162.0	118.90
S11	500	10	1.776	165.1	190.5	120.50
S12	450	10	0.769	66.40	77.30	87.600
S13	550	10	2.164	184.2	262.5	135.50
S14	500	5	0.956	117.8	165.4	111.20
S15	500	15	1.131	157.6	159.0	104.30
S16	550	0	1.789	139.6	213.2	98.030

3.2. Microhardness

Microhardness results at different operating temperatures and ZrO_2 volume fractions are listed in Table 3. The highest value of hardness was observed at 550 °C and 10 wt % of ZrO_2. With 5 wt % ZrO_2 addition and forging temperatures of 450 and 550 °C, hardness increased by 38.42% (S1 and S2). However, the hardness of S12 and S13 forged at 450 to 550 °C increased by 54.7% from 87.6 to 135.5 HV with 10 wt % ZrO_2 addition.

As shown in Table 3, the MH of the 100% chip sample (S16) was 98.03 HV, whereas the sample reinforced with 10 wt % ZrO_2 (S13) had the highest MH of 135.50 HV. The hardness increment was 38%, although both two samples (S13 and S16) were preheated at 550 °C. Sample S13 recorded the highest hardness of 135.5 HV, presenting the considerable effect of 10 wt % of ZrO_2 particles and 550 °C forging temperature. This result corresponds to the trend observed in the UTS results. Moreover, it has been demonstrated that increasing temperature above 500 °C contributed to increased strength due to finer particle dispersion (Arivazhagan, Mahalashmi and Boopathi, 2016; Shamsudin, Lajis, and Zhong, 2016). The hardness of 550 °C-preheated samples began to drop when the ZrO_2 content increased to 15 wt % (S4 and S8). The conglomeration of a high content of reinforcement particles causes porosity in composite material (Maniam *et al.*, 2020). The hardness increases linearly with temperature due to grain size reduction and refinement (Sabbar *et al.*, 2021; Rahimian *et al.*, 2009).

3.3. Modelling and optimization of the experimental factors for MMC performance

3.3.1 ANOVA of ultimate tensile strength and microhardness using RSM

The obtained UTS and MH data were used for further analyses by ANOVA and regression analysis. ANOVA and RSM were carried out to determine the significance of each factor considered in the experiment. The ANOVA results of the full factorial and curvature test suggested further optimization due to the positive effect of curvature. Therefore, four more experiments were added.

For data analysis, checking the goodness of the model's fit is required. The model adequacy checking includes regression model test for significance, model coefficients significance, and p-value of lack of fit test (Analyse it- Software, 2022). The well-developed chosen model should indicate an insignificant lack of fit. The coefficient of determination (R^2) reports how closely the model fitting to the experimental data. The R^2 values for both tensile strength and microhardness were 99% and 96% respectively, which were within the acceptable range ($\alpha = 0.05$, or 95% confidence). The p-value is applied to test the null hypothesis for each term when the coefficient has no effect (0). The p-value (<0.05) means that the null hypothesis is able to be rejected because the coefficient is likely not equal to zero. The ANOVA result in Tables 4 and 5 shows that the quadratic model is considered statistically significant for UTS and MH responses, except for Vf, 2-Way Interaction and TpVf terms. The calculated *p*-values of the model's rest terms, such as temperature (Tp) and ZrO_2 volume fraction (Vf), are less than 0.05, indicating that the model is statistically significant. Consequently, the model fits the experimental data, and input factors affect responses. The lack of fit value of 0.458 and 0.168 for TS and MH respectively is greater than 0.05, signifying that the model is non-significant relative to the noise and denoted a well-developed chosen model, as shown in Tables 4 and 5.

In UTS result analysis, R^2, adjusted R^2, and predicted R^2 have respective values of 0.9902, 0.9863, and 0.9769. The results prove the impact of zirconia particles on the TS of the developed composite. Meanwhile, the R^2, adjusted R^2, and predicted R^2 values for MH are 0.967, 0.949, and 0.8985, respectively (refer to Table 5). The R^2 value of 0.967 is close to 1, which explains the strong correlation between the experimental factors and output

responses. The predicted R^2 value of 0.8985 is in reasonable agreement with the adjusted R^2 value of 0.949, as shown in Table 5.

Table 4 Response Surface Regression: *TS* versus *Tp*, V_f ANOVA

Source	DF	Adj SS	Adj MS	*F* value	*p-value*	
Model	4	86517.3	21629.3	252.7	0.000	Significant
Linear	2	83113.6	41556.8	485.5	0.000	
Tp	1	83095.6	83095.6	970.8	0.000	
Vf	1	18.0000	18.0000	0.210	0.657	
Square	2	3403.70	1701.80	19.88	0.000	
Tp*Tp	1	636.300	636.300	7.430	0.021	
Vf*Vf	1	1453.50	1453.50	16.98	0.002	
Error	10	855.900	85.6000			
Lack-of-Fit	4	350.700	87.7000	1.04	0.458	Not significant
Pure Error	6	505.200	84.2000			
Total	14	87373.2				

Standard deviation = 0.09252, R^2 = 0.9902, R^2 adjusted = 0.9863, R^2 predicted = 0.97693

DF is the degree of freedom, Adj SS is the adjacent sum of squares, Adj MS is the adjacent mean squares, and *p-value* is level of significance.

Table 5 Response Surface Regression: MH versus Tp, Vf ANOVA

Source	DF	Adj SS	Adj MS	*F* value	*p* value	
Model	5	5158.0	1031.6	52.72	0.000	Significant
Linear	2	4085.9	2042.7	104.41	0.000	
Tp	1	4067.0	4067.0	207.85	0.000	
Vf	1	18.850	18.850	0.9600	0.352	
Square	2	954.85	477.43	24.400	0.000	
Tp*Tp	1	185.43	185.43	9.4800	0.013	
Vf*Vf	1	399.03	399.00	20.390	0.001	
2-Way Interaction	1	117.27	117.20	5.9900	0.037	
Tp*Vf	1	117.27	117.20	5.9900	0.037	
Error	9	176.11	19.570			
Lack-of-Fit	3	95.810	31.940	2.3900	0.168	Not significant
Pure Error	6	80.300	13.380			
Total	14	5334.0				

Standard deviation = 0.04423, R^2 = 0.967, R^2 adjusted = 0.949, R^2 predicted = 0.8985

3.3.1.1 The adequacy of the models with significant terms

Pareto charts of the standardized effects in Figure 3 (a) and (b) illustrate that the main influence factors on the responses are Tp and then Vf, where TP and Vf are denoted by the A and B, respectively. The two-level interaction is significant model term as well. However, the operating temperature (A) is the most outstanding factor influencing the UTS and MH. The other factors that exceed the reference line are insignificant factors.

Figure 4 (a) and (b) show the residual plots for TS and MH. The bell-shaped and systematic residuals histogram in the TS graph proves that the ZrO_2 volume fraction for the center is normally distributed and well fit. The normal probability plot of the residuals is very close to the straight line. Therefore, the errors are minor and normally distributed. The randomly scattered points reveal the equal distribution and constant variance. The interaction between temperature and volume fraction has significant effects on TS and MH responses.

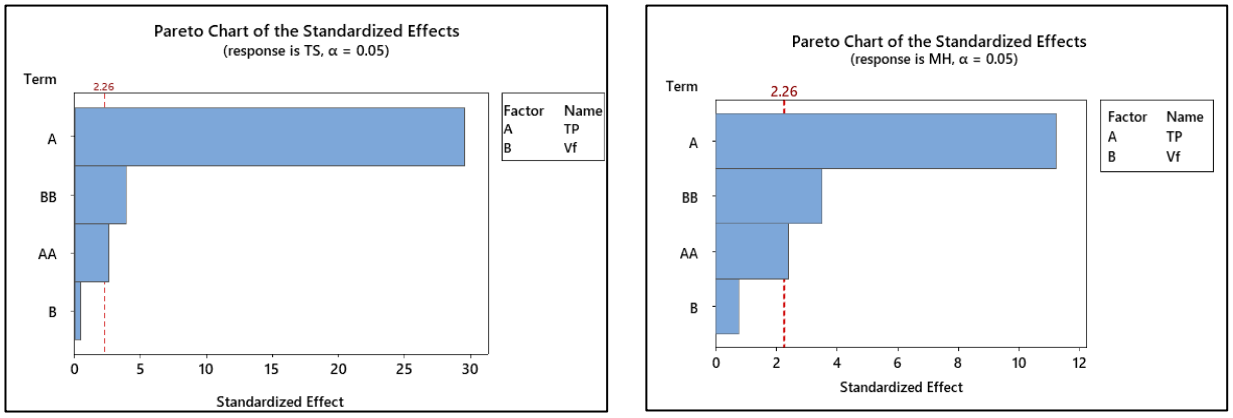

(a) (b)

Figure 3 (a) Pareto chart of the standardized effects of TS response and (b) Pareto chart of the standardize effects for MH

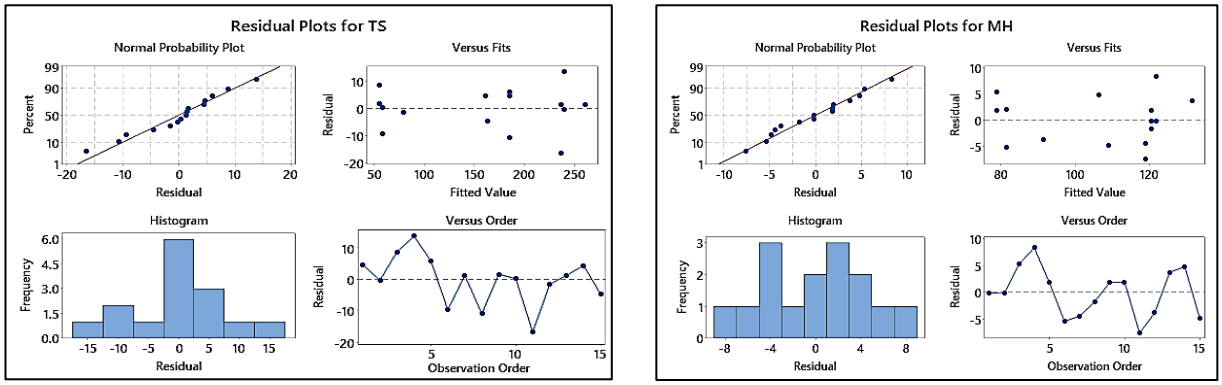

(a) (b)

Figure 4 (a) Residual plots for UTS and (b) MH Residual plots

3.3.2 Developing Empirical Model

The final regression model was constructed using Minitab 18 to predict TS and MH of the composite as expressed in equations 8 and 9.

$$TS = -2327 + 7.85\,T_P + 18.50\,V_f - 0.00603\,(T_P)^2 - 0.911\,(V_f)^2 \quad (8)$$

$$MH = -869 + 3.51\,T_P + 2.17\,V_f - 0.00326\,(T_P)^2 - 0.478\,V_f + 0.01532\,T_P\,V_f \quad (9)$$

Linear regression analysis identifies correlations between response and predicted variables. Both equations indicate that temperature has more effect than ZrO_2.

3.3.3 Optimization

The RSM was used to optimize UTS and MH by analyzing the input factors to acquire the optimal values that result in maximum UTS and MH. According to RSM optimization results 550 °C and 10.1515 wt% are the optimal parameters yielding maximum TS and MH values of 261.53 MPa and 132.4 HV, respectively. The Optimized solution is consistent with experimental results of 262.5 MPa and 135.5 HV.

Table 6 Optimization Result for UTS and MH

Parameter	Level			Maximum Responses	
	High	Optimal	Low	TS (MPa)	MH(HV)
Tp (°C)	550	550	450	261.53	132.4
Vf (wt %)	15	10.15	5		

3.4. Confirmation Test and Validation

Three confirmation tests were performed for empirical result validation. The specimens were prepared based on optimal parameters settings of 550 °C and 10.15 wt %. to validate the quadratic regression model. The average error between the experimental value and the predicted model is less than 2%. The predicted and measured UTS agreed well, thus results confirm the reproducibility of the experimental data.

Table 7 Results of the Experimental Validation

Exp. No.	UTS (MPa)		
	Predicted	Experimental	Error (%)
S1	261.53	252.0	3.6
S2		258.0	1.35
S3		263.6	0.8
Average		257.87	1.9

3.5. Microstructural and Fracture Surface Examination

The examination was carried out on specimens produced from different parameter settings as presented in Table 8. The intercept process calculates the G Number by superimposing a pattern on an image and counting the number of times it intersects with the grain boundary. The measurement of average grain size using the intercept method was based on ASTM E112-13 (2013) standard.

S0 (unreinforced sample) has a relative value in grain area and diameter growth, as seen in 8. S1 possessed a low YS of 55.89 MPa (Table 3) and showed the lowest grain area and diameter. The grain size affects the yield strength (Hall–Petch equation). The grain size was coarse due to the low forging temperature (450 °C). The 550 °C-heated/10 wt %-reinforced sample (S3) possessed a slightly smaller grain area and diameter. In other words, at recrystallization temperature, the grain boundary becomes finer with a smaller grain. The smaller the grain size, the greater the ductility, yield strength, and tensile strength. A smaller grain creates more impediments per unit area of the slip plane.

Table 8 Result of Grain Size Measurement

Sample no.	Temp. (°C)	ZrO_2 (wt%)	G No.	Average grain area (μm²)	Average. Diameter (μm)
S1	450	5	5.07	3866.66	62.086
S2	500	15	5.04	3937.52	62.692
S3	550	10	5.01	3828.38	62.298
S0	550	0	5.02	3984.76	63.096

Figure 5 (a–c) of SEM micrographs shows a fracture surface of the tensile profiles for sample S1 forged at 450 °C and reinforced with 5 wt % ZrO_2. Sample S1 possessed the lowest YS of 55.89 MPa (Table 3). Surface morphology was visualized utilizing SEM (Hitachi SU1510). Prominent crack ridge and periphery coarse topography appear in Figure 5b. The low temperature and volume fraction led to poor chip bonding, revealing long cracks and ridges instead of equiaxed dimples. The partial oxide layer destruction between chips impeded complete welding and indicated the effect. It is related to oxidation between layers and chip boundaries, preventing grain growth due to chip boundaries (Parveen, Chauhan, and Suhaib, 2019).

Figure 5 (d–f) shows the fracture surface topography of S13: 550 °C-preheated and 10 wt % ZrO_2. The sample demonstrated the highest UTS of 262.52MPa. The positive influence of high temperature is proven in the sample fracture mechanism. The crack initiation zone at 70× magnification is characterized by periphery coarse and quasi-cleavage, as depicted in Figure 5 (e). Microvoids and dimples indicated a ductile fracture mode. Numerous small

dimples demonstrated the effect of high temperature and volume fraction on the behavior of fracture surfaces. The coalescence occurs when reinforced material elongates to initial spaces leading to a dimpled appearance Figure 5 (f). However, the dimples were not uniformly formed; some differences in size were apparent.

Figure 6 (a–d) of SEM micrographs depicts a fracture surface of tensile profiles for S0 (non-reinforced specimen) with 550 °C and 0 wt % ZrO_2. This sample was prepared from pure chips (without reinforcement) to study the fracture behavior differences between ZrO_2-reinforced and non-reinforced specimens. The top view of the fracture surface is characterized by the morphology of primary and secondary cracks, as shown in (a). The crack propagation in Figure 6 (e) started from the weakest points of the chip boundaries due to the precipitation and the chip's large surface required high consolidation. The interfacial bonding between Al-chip and ZrO_2 reinforced material minimizes the porosity as prominent in SEM images shown in Figure 6 (f). Microvoids are visible in some regions in Figure 6 (d), indicating the ductility of recycled material.

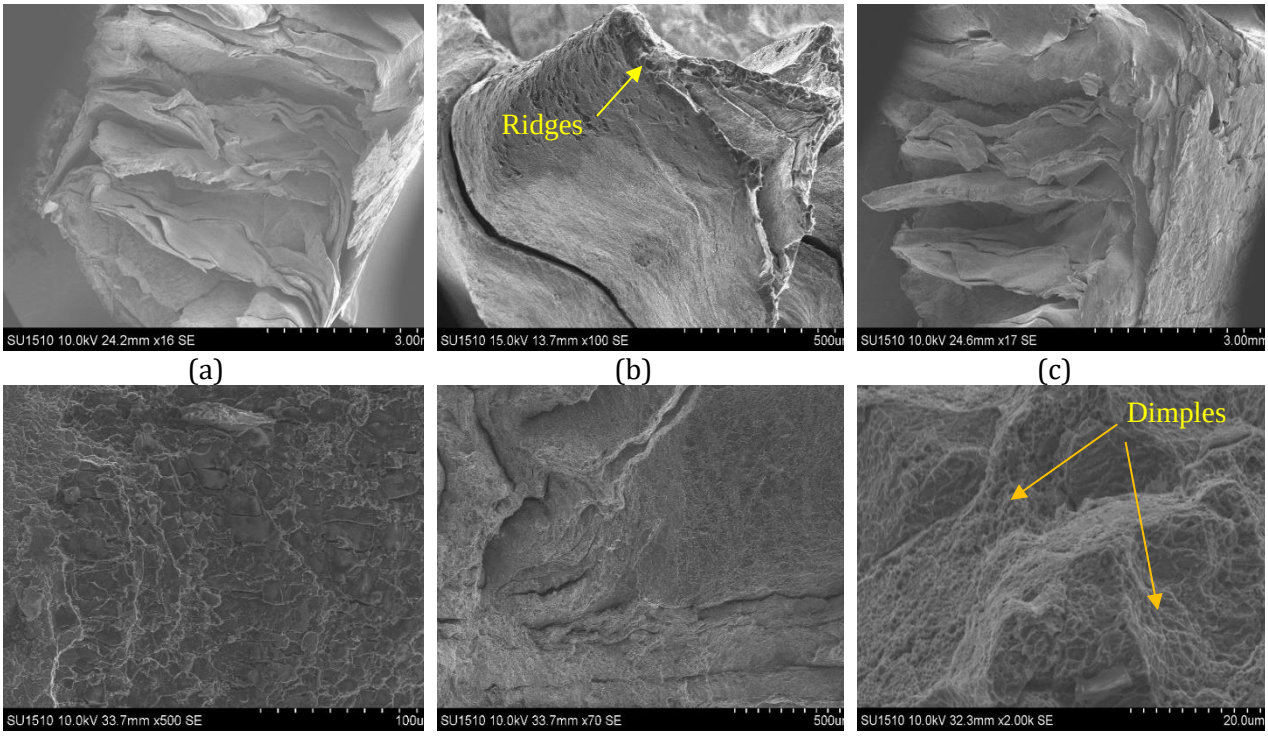

(a) (b) (c)

(d) (e) (f)

Figure 5 SEM micrographs of the tensile profiles for 450 °C, 5 wt % ZrO_2 (S1): (a) an overview of the brittle fracture surface, (b) the quasi-cleavage fracture surface, (c) the observed ridges, and SEM micrographs of tensile profiles for 550 °C, 10 wt % ZrO_2 (S13): (d) homogeneous distribution of ZrO_2 in matrix, (e) the cleavage facet and crack topology and (f) fine equiaxed dimples

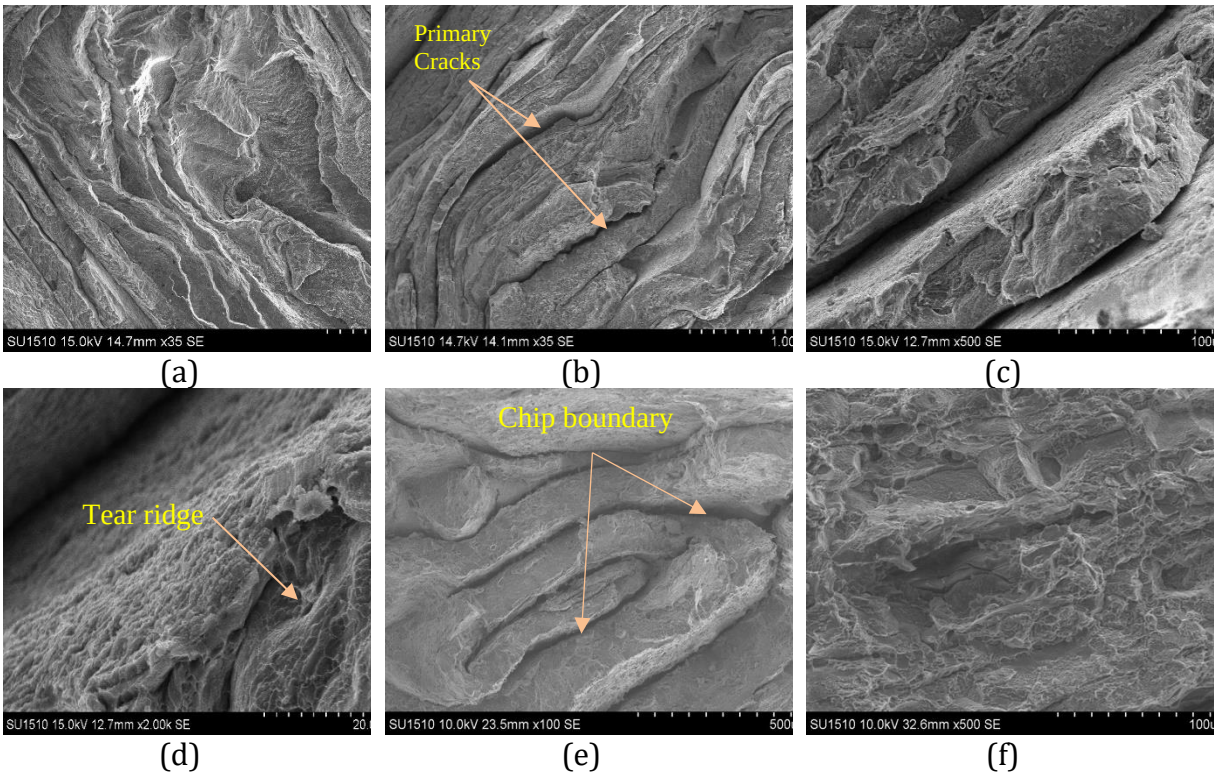

Figure 6 SEM micrographs of the tensile profiles for 550 °C, 0 wt % ZrO_2 (S0): (a) an overview of the fracture surface, (b) the cracks on the chip boundary at 35× and (c) 500×, (d) cleavage-like and dimples, (e) cracks on the chip boundary and (f) microvoids appearance at 500×

3.6. Analysis of Relative Density

As shown in Figure, the lowest density of 2.74 g/cm^3 was attained at 450 °C, 15 wt % ZrO_2, while the 550 °C, 10 wt % sample recorded the highest density of 2.83 g/cm^3. The density increased by 2.47%, from 2.76 to 2.8281 g/cm^3, when the forging temperature was varied from 450 to 550°C with a fixed 10 wt % ZrO_2. Although the samples were cold-compressed at the same 35 ton pressure, the higher temperature made a difference in reducing voids, as supported by UTS results. Additionally, the zirconia's high density of 5.68 g/cm^3 contributes to improving the total density of composite material (Al-Alimi *et al.*, 2020). The higher obtained density was 2.83 g/cm^3, close to the density of AA7075-T6 (2.81 g/cm^3). The density of 0wt% ZrO_2 sample S16 is 2.76 g/cm^3, whereas the density of 15wt% ZrO_2 sample S8 is 2.8 g/cm^3. However, both two samples were forged at 550 °C, the increment was relative to 1.44%. This is due to the higher density of zircon compared to aluminum (Loong and Lajis, 2015).

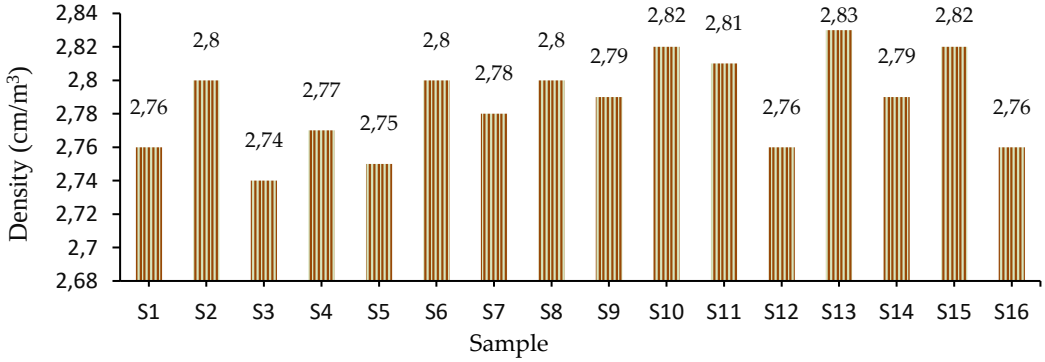

Figure 7 The density measurement of samples

4. Conclusions

The maximum UTS of 262.5 MPa was obtained with 10 wt % ZrO_2 + 90% chip at 550°C, showing 23.18% higher UTS than the 100% chip sample. However, UTS began to drop when the volume fraction of ZrO_2 exceeded 10 wt %. The highest microhardness of 135.5 HV was attained with 10 wt % ZrO_2 and 550°C. The density increased from 2.76 to 2.83 g/cm^3, by increasing the processing temperature from 450 to 550 °C for the sample with 10 wt % ZrO_2. The average grain diameter increased with operating temperature and decreased with increasing ZrO_2 content above 10%. SEM micrograph revealed a uniform distribution of ZrO_2 particles in the matrix. ANOVA with RSM analysis revealed that TP was the most influential factor in UTS and MH responses. However, Vf had a considerable effect on responses as well. The optimization results suggested 550°C and 10.15 wt% as optimal parameter settings for maximum UTS and MH. The average error between experimental and predicted optimal results was 1.9%, indicating a high correlation. The reinforcement material and chip morphology should be studied further in order to improve composite quality and expand its application limits.

Acknowledgments

Communication of this research is made possible through monetary assistance by Universiti Tun Hussein Onn Malaysia and the UTHM Publisher's Office via Publication Fund E15216. The authors express their profound appreciation for the supplementary provisions provided by Sustainable Manufacturing and Recycling Technology, Advanced Manufacturing and Materials Center (SMART-AMMC), Universiti Tun Hussein Onn Malaysia.

References

Agboola, O., Babatunde, D.E., Isaac Fayomi, O.S., Sadiku, E.R., Popoola, P., Moropeng, L., Yahaya, A., Mamudu, O.A., 2020. A Review on The Impact of Mining Operation: Monitoring, Assessment and Management. *Results in Engineering*, Volume 8, p. 100181

Al-Alimi, S.A.M., Lajis, M.A. bin, Shamsudin, S. bin. Long, C.B., 2022. Influence Of Zirconia Percent On Physical Properties Of Zirconia - Aluminum Chip Matrix (Al6061) Nanocomposites. *Journal of Nanostructures*, Volume 12(1), pp. 194–203

Analyse it- Software, 2022. The Lack of Fit F-test STAT 501. Available online at: https://online.stat.psu.edu/stat501/lesson/2/2.11, Accessed on August 10, 2022

Arivazhagan, K., Mahalashmi, S., Boopathi, D.L., 2016. Evaluation on Recycling of E-Waste Aluminium In Metal Matrix Composite. *International Research Journal of Engineering and Technology,* Volume 3(4), pp. 2822–2829

ASTM E8/E8M-21, 2022. Standard Test Methods for Tension Testing of Metallic Materials. Available online at: https://www.astm.org/e0008_e0008m-21.html, Accessed on August 3, 2022

Cui, J., Roven, H.J., 2010. Recycling of Automotive Aluminum. *Transactions of Nonferrous Metals Society of China,* Volume 20(11), pp. 2057–2063

Dhanesh, S., Kumar, K.S., Fayiz, N.KM., Yohannan, L., Sujith, R., 2021. Recent Developments in Hybrid Aluminium Metal Matrix Composites: A Review. *Materials Today: Proceedings,* Volume 45(part 2), pp. 1376–1381

International Aluminium Institute, n.d. Aluminium Sector Greenhouse Gas Pathways to 2050. Available online at: https://international-aluminium.org/resource/aluminium-sector-greenhouse-gas-pathways-to-2050-2021/, Accessed on August 13, 2022

Jankovic, A., Chaudhary, G., Goia, F., 2021. Designing The Design of Experiments (DOE) – An Investigation on The Influence of Different Factorial Designs on The Characterization of Complex Systems. *Energy and Buildings*, Volume 250, p. 111298

Keoleian, G.A., Sullivan, J.L., 2012. Materials Challenges and Opportunities for Enhancing the Sustainability of Automobiles. *MRS Bulletin*, Volume 37(4), pp. 365–372

Lajis, MA., Yusuf, N. K., Ahmad, A., 2018. Life Cycle Assessment on The Effects of Parameter Setting In Direct Recycling Hot Press Forging of Aluminum. *Materials Science Forum*, Volume 923, pp. 143–148

Loong, C.B., Lajis, M.A., 2015. Direct Recycling of Aluminium 6061 Chip Through Cold Compression. *International Journal of Mechanical & Mechatronics Engineering,* Volume 15(4), pp. 43–47

Maniam, B.S., Purusothaman, V.R., Karuppusamy, S.M., Ganesh, S.H., Dan, R.K.M., Subramaniam, B., Purusothaman, V.R., Markandan, R.K., 2020. Review On Properties of Aluminium Metal Matrix Composites. *Journal of Mechanical and Energy Engineering*, Volume 4(44), pp. 57–66

Parveen, A., Chauhan, N.R., Suhaib, M., 2019. *Mechanical and Tribological Behaviour of Al-ZrO2 Composites: A Review.* Part of Lecture Notes in Mechanical Engineering Book Series. Springer: Singapore

Rahimian, M., Ehsani, N., Parvin, N., Baharvandi, H., Reza, 2009. The Effect of Particle Size, Sintering Temperature and Sintering Time on The Properties of Al-Al2O3 Composites, Made By Powder Metallurgy. *Journal of Materials Processing Technology*, Volume 209(14), pp. 5387–5393

Rana, RS., Purohit, R., Das, S., 2012. Reviews on The Influences of Alloying Elements on The Microstructure and Mechanical Properties of Aluminum Alloys and Aluminum Alloy Composites. *International Journal of Scientific and Research Publications*, Volume 2(6), pp. 1–7

Reddy, M.S.P., Raju, H.P., Banapurmath, N., Meti, V.K.V., 2020. Influence of ZrO2 Nano Particles on The Behavior of Mechanical and Tribological Properties of the AA7075 Composite. *The Journal of Nanomaterials, Nanoengineering and Nanosystems*, Volume 236(1–2), pp. 55–62

Sabbar, H.M., Leman, Z., Shamsudin, S., Tahir, S.M., Jaafar, C.N.A., Ariff, A.H.M., Zahari, N.I., Rady, M.H., 2021. The Effect of Solid-State Processes and Heat Treatment on The Properties of aa7075 Aluminum Waste Recycling Nanocomposite. *Materials*, Volume 14(21), p. 6667

Shamsudin, S., Lajis, M.A., Zhong, Z.W., 2016. Solid-State Recycling of Light Metals: A Review. *Advances in Mechanical Engineering*, Volume 8(8), pp. 1–23

Srivyas, P.D., Charoo, M.S., 2018. Aluminum Metal Matrix Composites Review of Reinforcement; Mechanical Behavior. *International Journal of Engineering & Technology*, Volume 7(2.4), pp. 117–122

Wan, B., Chen, W., Lu, T., Liu, F., Jiang, Z., Mao, M., 2017. Review of Solid State Recycling Of Aluminum Chips. *Resources, Conservation and Recycling*, Volume 125, pp. 37–47

Yong, Z.J., Bashir, M.JK., Ng, C.A., Sethupathi, S., Lim, J.W., Show, P.L., 2019. Sustainable Waste-to-Energy Development in Malaysia. *Processes,* Volume 7, p. 676